



Influence of Meteorology and interrelationship with greenhouse gases (CO₂ and CH₄) at a suburban site of India

Gaddamidi Sreenivas, Pathakoti Mahesh, Jose Subin, Asuri Lakshmi Kanchana, Pamaraju Venkata Narasimha Rao, and Vinay Kumar Dadhwal

Atmospheric and Climate Sciences Group (ACSG), Earth and Climate Science Area (ECSA), National Remote Sensing Center (NRSC), Indian Space Research Organization (ISRO), Hyderabad, 500037, India

Correspondence to: Pathakoti Mahesh (mahi952@gmail.com)

Received: 28 October 2015 – Published in Atmos. Chem. Phys. Discuss.: 4 December 2015

Revised: 14 March 2016 – Accepted: 15 March 2016 – Published: 24 March 2016

Abstract. Atmospheric greenhouse gases (GHGs), such as carbon dioxide (CO₂) and methane (CH₄), are important climate forcing agents due to their significant impacts on the climate system. The present study brings out first continuous measurements of atmospheric GHGs using high-precision LGR-GGA over Shadnagar, a suburban site of Central India during the year 2014. The annual mean CO₂ and CH₄ over the study region are found to be 394 ± 2.92 and 1.92 ± 0.07 ppm ($\mu \pm 1\sigma$) respectively. CO₂ and CH₄ show a significant seasonal variation during the study period with maximum (minimum) CO₂ observed during pre-monsoon (monsoon), while CH₄ recorded the maximum during post-monsoon and minimum during monsoon. Irrespective of the seasons, consistent diurnal variations of these gases are observed. Influences of prevailing meteorology (air temperature, wind speed, wind direction, and relative humidity) on GHGs have also been investigated. CO₂ and CH₄ show a strong positive correlation during winter, pre-monsoon, monsoon, and post-monsoon with correlation coefficients (R_s) equal to 0.80, 0.80, 0.61, and 0.72 respectively, indicating a common anthropogenic source for these gases. Analysis of this study reveals the major sources for CO₂ are soil respiration and anthropogenic emissions while vegetation acts as a main sink, whereas the major source and sink for CH₄ are vegetation and presence of hydroxyl (OH) radicals.

1 Introduction

The Intergovernmental Panel on Climate Change (Stocker et al., 2013) reported that humankind is causing global warming through the emission of greenhouse gases (GHGs), particularly carbon dioxide (CO₂) and methane (CH₄). CO₂ and CH₄ concentrations, have increased by 40 and 150 % respectively since pre-industrial times, mainly from fossil fuel emissions and secondarily from net land use change emissions (Stocker et al., 2013; Huang et al., 2015). CO₂ measurements at Mauna Loa, Hawaii (Monastersky, 2013) have exceeded the 400 ppm mark several times in May 2013. CH₄ is also receiving increasing attention due to high uncertainty in its sources and sinks (Keppler et al., 2006; Miller et al., 2007; Frankenberg et al., 2008). Kirschke et al. (2013) reported that in India, agriculture and waste constitute the single largest regional source of CH₄. Although many sources and sinks have been identified for CH₄, their relative contribution to atmospheric CH₄ is still uncertain (Garg et al., 2001; Kirschke et al., 2013). In India, electric power generation contributes to half of India's total CO₂ equivalent emissions (Garg et al., 2001).

Arid and semi-arid areas comprise about 30 % of the Earth's land surface. Climate change and climate variability will likely have a significant impact on these regions (Huang et al., 2008, 2015). The variability of environmental factors may result in significant effects on regional climate and global climate (Wang et al., 2010), especially the radiative forcing, via the biogeochemical pathways affecting the terrestrial carbon cycle. Global climate change has serious impacts on humans and ecosystems. Due to this, many factors have been identified that may reflect or cause varia-

tions in environmental change (Pielke et al., 2002). Out of these, the Normalized Difference Vegetation Index (NDVI) has become one of the most widely used indices to represent the biosphere influence on global change (Liu et al., 2011). Greenhouse and other trace gases have great importance in atmospheric chemistry and for radiation budget of the atmosphere–biosphere system (Crutzen, 1991). Hydroxyl radicals (OH) are very reactive oxidizing agents, which are responsible for the oxidation of almost all gases that are emitted by natural and anthropogenic activities in the atmosphere. Atmospheric CO₂ measurements are very important for understanding the carbon cycle because CO₂ mixing ratios in the atmosphere are strongly affected by photosynthesis, respiration, oxidation of organic matter, biomass and fossil fuel burning, and air–sea exchange process (Machida et al., 2003).

The present study brings out first continuous measurements of atmospheric GHGs using high-precision LGR-GGA over Shadnagar, a suburban site of Central India during the year 2014. In addition to GHG observations, we have also made use of an automatic weather station (AWS) data along with model/satellite-retrieved observation during the study period. Details about study area and data sets are described in the following sections.

2 Study area

Shadnagar is situated in the Mahabubnagar district of the newly formed Indian state of Telangana. It is a suburban location situated ~70 km away from the urban site of Hyderabad (northern side) with a population of ~0.16 million (Patil et al., 2013). A schematic map of study area is shown in Fig. 1a. Major sources of pollutants over Shadnagar can be from small- and medium-scale industries, biomass burning, and bio-fuel as well as from domestic cooking. In the present study, sampling of GHGs and related meteorological parameters is carried out in the premises of the National Remote Sensing Center (NRSC), Shadnagar Campus (17°02' N, 78°11' E). A national highway and railway track (non-electrified) are to the east of the sampling site at an aerial distance of approximately 2.25 km.

Mean monthly variations of temperature (°C) and relative humidity (RH %) observed at Shadnagar during 2014 are shown in Fig. 1e and d respectively. The Indian Meteorological Department defined monsoon as June–July–August–September, JJAS), post-monsoon (October–November–December, OND), winter (January–February, JF), and pre-monsoon (March–April–May, MAM) seasons in India. Temperature over Shadnagar varies from ~20 to ~29°C. RH in Shadnagar reached a maximum of ~82% in monsoon from a minimum of ~48% recorded during pre-monsoon. Surface wind speed (Fig. 1c) varies between 1.3 and 1.6 m s⁻¹ with a maximum observed during monsoon and minimum in pre-monsoon. The air mass advecting

(Fig. 1b) towards the study site is either easterly or westerly. The easterly wind prevails during winter and gradually shifts to south-westerlies in pre-monsoon, and it dominates during monsoon.

3 Data set and methodology

Details about the instrument and data utilized are discussed in this section. The availability and frequency of the observations of all data used in present study are tabulated in Table 1.

3.1 In-situ observations

3.1.1 Greenhouse Gas Analyser (GGA)

The Los Gatos Research's Greenhouse Gas Analyser (model: LGR-GGA-24EP) is an advanced instrument capable of simultaneous measurements of CO₂, CH₄, and H₂O. This instrument is well known for high precision and accuracy, both of which are crucial for understanding background concentrations of atmospheric GHGs, with specifications meeting WMO standards of measurement (Berman et al., 2012; Shea et al., 2013; Mahesh et al., 2015). It is based on enhanced off-axis integrated cavity output spectroscopy (OA-ICOS) technology (Paul et al., 2001; Baer et al., 2002), which utilizes true wavelength scanning to record fully resolved absorption line shapes. Considering the nature of the site, flow rate is fixed at 7 L min⁻¹. Ambient air entering the GGA is analysed using two near-infrared distributed feedback tunable diode lasers: one for a CO₂ absorption line near 1.60 μm ($\nu_0 = 6250 \text{ cm}^{-1}$) and the other to probe CH₄ and H₂O absorption lines near 1.65 μm ($\nu_0 = 6060.60 \text{ cm}^{-1}$). The concentration of the gases is determined by the absorption of their respective characteristic absorption lines with a high sampling time of 1 sec. A detailed explanation regarding the configuration, working, and calibration procedure performed for GGA in NRSC can be found elsewhere in Mahesh et al. (2015). In the present study we used GGA retrieve CO₂ and CH₄ data. High-resolution data sets are diurnally averaged and used in further analysis. Due to the failure of internal central processing unit of the analyzer, data are not recorded from pre-monsoon month of 1 May to 18 June during the study period.

3.1.2 O₃ and NO_x analyzer

Surface concentrations of O₃ and NO_x have been measured continuously using online analyzers (model nos. 49i and 42i for O₃ and NO_x respectively) from Thermo Scientific, USA, since July 2014. The trace gas (O₃ and NO_x) sampling inlet is installed on the top of a 2 m mast fixed on the roof of an 8 m high building, and ambient air flow is supplied to the instruments. The inlet prevents the ingress of rain water and is equipped with 0.5 μm filter to prevent accumulation of dust within the instrument. The ozone analyzer is based

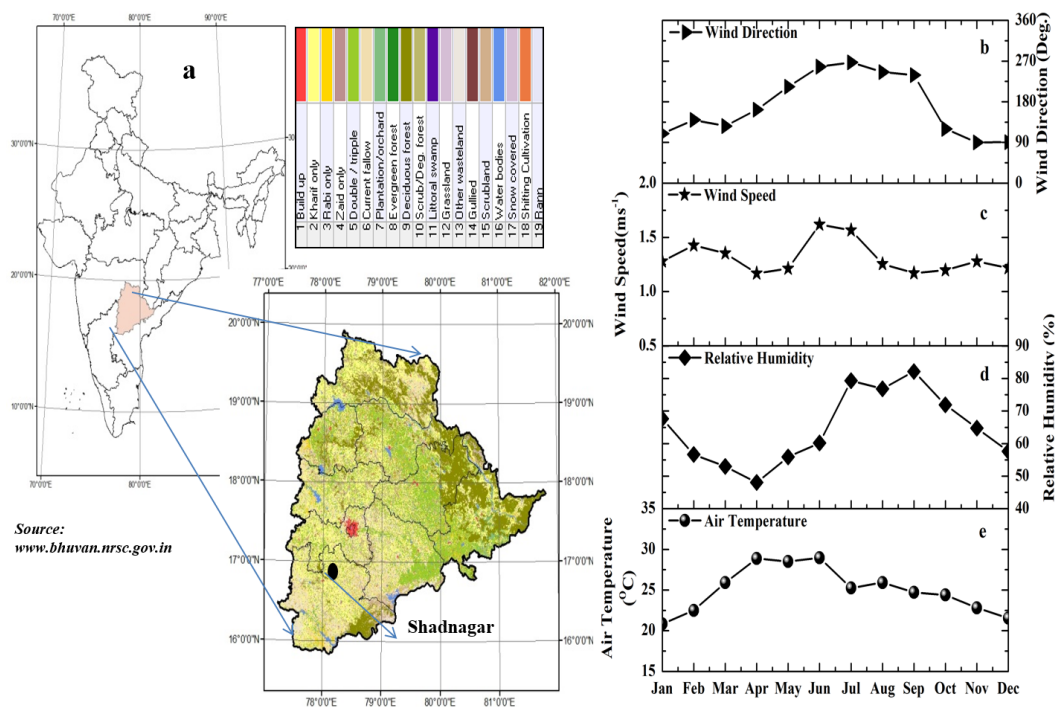


Figure 1. (a) Schematic representation of study area; (b–e) seasonal variation of prevailing meteorological conditions during 2014.

Table 1. Data used.

Sensor	Period	Parameter	Resolution	Source
GGA-24EP	Jan 2014 to Dec 2014	CO ₂ , CH ₄ , and H ₂ O	1 Hz time	ASL,NRSC
42i-NO-NO ₂ -NO _x	Jul 2014 to Sep 2014	NO _x (= NO + NO ₂)	1 min time	ASL,NRSC
49i-O ₃	Jul 2014 to Sep 2014	O ₃	1 min time	ASL,NRSC
AWS	Jan 2014 to Dec 2014	WS, WD, AT, RH	60 min time	NRSC
Terra/MODIS	Jan 2014 to Dec 2014	NDVI	5 km horizontal	http://ladsweb.nascom.nasa.gov/data/search.html
COSMIC-1DVAR	Jul 2013 to Jun 2014	Refractivity (<i>N</i>)	0.1 km vertical	
HYSPLIT	Jan 2014 to Dec 2014	Backward trajectory	5 day isentropic model (1 to 4 km)	http://ww.arl.noaa.gov/ready/hysplit4.html
FEER v1	Jan 2013 to Dec 2013	Fire radiative power (FRP)		http://ladsweb.nascom.nasa.gov/data/search.html

on Beer–Lambert–Bouguer law which relates absorption of light to the concentration of species as its operating principle and has an in-built calibration unit for conducting periodical span and zero checks. The NO_x analyzer utilizes a molybdenum converter to convert NO₂ into NO and estimates the NO_x concentration by the intensity of light emitted during the chemiluminescent reaction of NO with O₃ present in the

ambient air. The analyzer is integrated with zero and span calibrations which are performed twice monthly.

Simultaneous observations of meteorological parameters are obtained from an AWS installed in NRSC, Shadnagar campus as a part of Calibration and Validation (CAL/VAL) project in March 2012 is equipped with nine sensors to measure 15 weather parameters. Weather parameters measured are at surface level and height of the AWS mast is ~ 10 m.

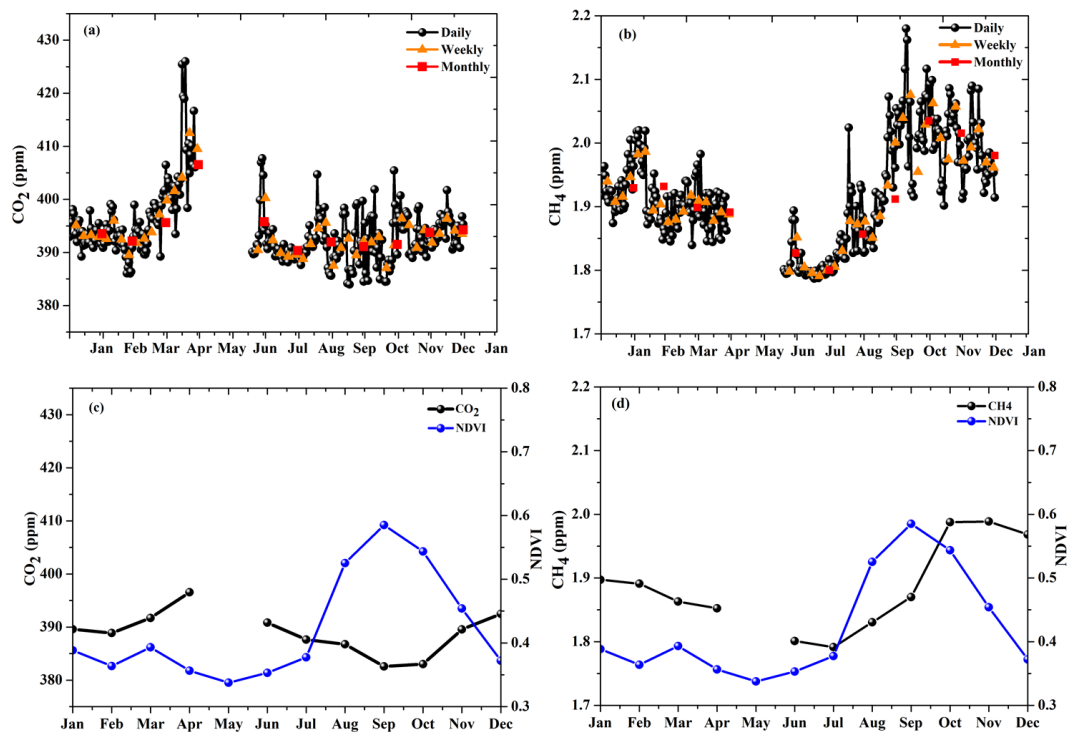


Figure 2. (a–b) Temporal variations of CO₂ and CH₄; (c–d) seasonal variations of CO₂ and CH₄ in conjunction with NDVI (Normalized Difference Vegetation Index) during 2014.

3.2 Satellite and model observations

3.2.1 Moderate-resolution Imaging Spectrometer (MODIS)

The MODIS was launched in December 1999 on the polar-orbiting NASA-EOS Terra platform (Salomonson et al., 1989; King et al., 1992). It has 36 spectral channels and acquires data in three spatial resolutions of 250, 500, and 1 km (channels 8–36), covering the visible, near-infrared, shortwave infrared, and thermal-infrared bands. In the present study we used monthly NDVI data obtained from Terra/MODIS at 5 km spatial resolution. The NDVI value is defined as the following ratio of albedos (α) at different wavelengths:

$$NDVI = \frac{\alpha_{0.86\mu\text{m}} + \alpha_{0.67\mu\text{m}}}{\alpha_{0.86\mu\text{m}} - \alpha_{0.67\mu\text{m}}} \quad (1)$$

NDVI values can range from -1.0 to 1.0 but typical ranges are from 0.1 to 0.7 , with higher values associated with greater density and greenness of plant canopies. More details of the processing methods used in generating the data set can be found in James and Kalluri (1994).

Table 2. Statistical correlation between CO₂ and CH₄.

Season no.	Season	Correlation coefficient (R)	Slope ($\frac{Y_{\text{CH}_4} \text{ (ppm)}}{X_{\text{CO}_2} \text{ (ppm)}}$)	ψ_{slope} (ppm)	$\Psi_{y\text{-int}}$ (ppm)
1	Monsoon (JJAS)	0.61	0.005	0.00015	1.91
2	Post-monsoon (OND)	0.72	0.0065	0.00014	1.52
3	Winter (JF)	0.80	0.0085	0.00018	9.13
4	Pre-monsoon (MAM)	0.80	0.0059	0.00021	2.73

3.2.2 Constellation Observation System for Meteorology, Ionosphere and Climate radio occultation (COSMIC-RO)

COSMIC is a GPS (Global Positioning System) RO observation system (Wang et al., 2013). It consists of six identical microsatellites and was launched successfully on 14 April 2006. GPS RO observation has the advantage of near-global coverage, all-weather capability, high vertical resolution, high accuracy, and self-calibration (Yunck et al., 2000). Geophysical parameters (such as temperature and humidity profiles) have been simultaneously obtained from re-

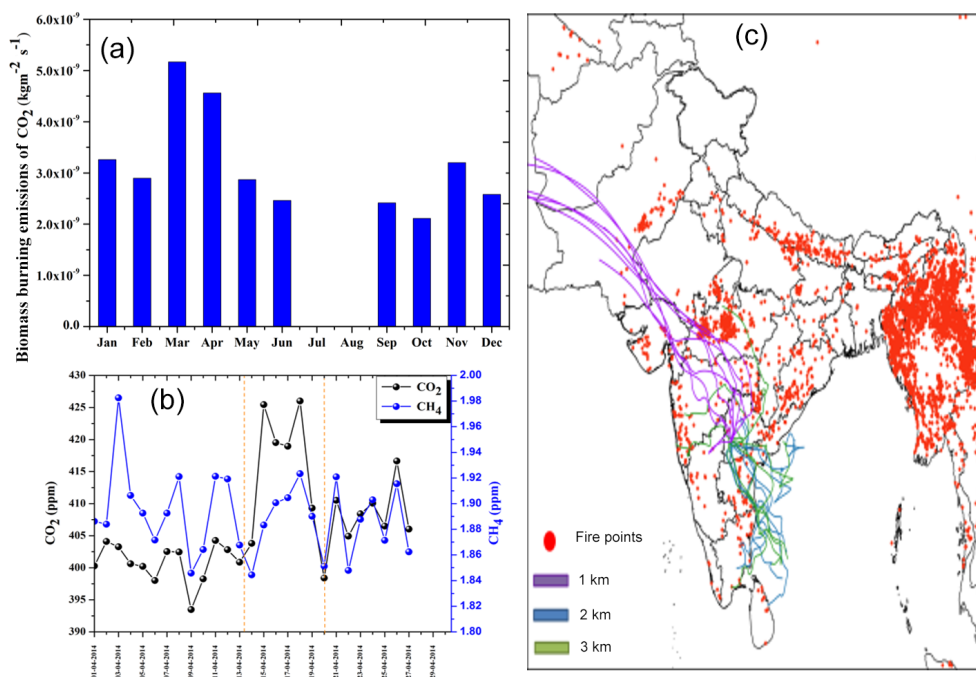


Figure 3. (a) Long term analysis of CO₂ biomass burning emissions over the study region; (b) biomass signatures on CO₂ / CH₄ during 14–21 April 2014 (a case study); (c) spatial distribution of MODIS-derived fire counts over Indian region during 14–21 April 2014.

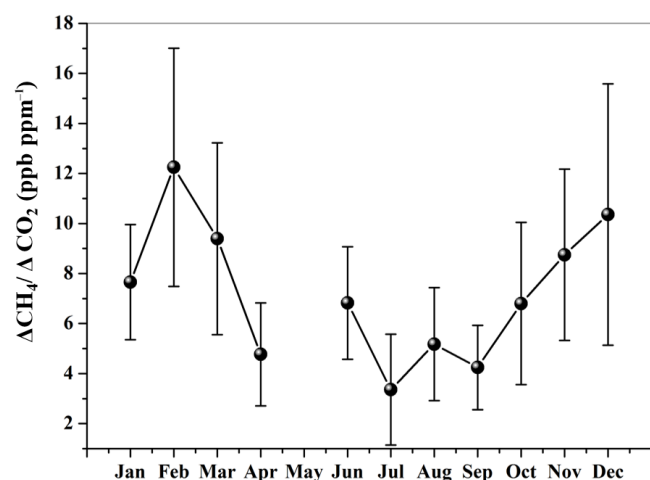


Figure 4. Monthly variation of $\Delta\text{CH}_4 / \Delta\text{CO}_2$ during the study period.

fractivity data using one-dimensional variational (1DVAR) analysis. Further COSMIC-RO profiles are used to estimate planetary boundary layer height (BLH). BLH is defined to be the height at which the vertical gradient of the refractivity or water vapour partial pressure is minimum. Ao et al. (2012) explained a detail methodology for calculating the BLH from refractivity (N). The planetary boundary layer (PBL) is part of the atmosphere closest to the Earth's surface where turbulent processes often dominate the vertical redistribution of

sensible heat, moisture, momentum, and aerosols/pollution (AO et al., 2012).

3.2.3 HYSPLIT model

The general air mass pathway reaching over Shadnagar is analysed using the HYSPLIT model (Draxler and Rolph, 2003; <http://www.arl.noaa.gov/ready/hysplit4.html>). We computed 5-day isentropic model backward air mass trajectories for all study days with each trajectory starting at 00:60 UTC and reaching the study site (Shadnagar) at different altitudes (1, 2, 3, and 4 km). Even though the trajectory analysis have inherent uncertainties (Stohl, 1998), they are quite useful in determining long-range circulation.

4 Results and discussion

4.1 Seasonal variations of CO₂ and CH₄

Temporal variations of CO₂ and CH₄ during the study period are shown in Fig. 2a and b. The circles indicate the daily mean, while triangular markers represent weakly averages and monthly mean by square markers. Annual mean of CO₂ over the study region is found to be 394 ± 2.92 (mean (μ) \pm standard deviation (1σ)) ppm with an observed minimum in monsoon and maximum in pre-monsoon. Seasonal mean values of CO₂ observed during different seasons are 393 ± 5.60 , 398 ± 7.60 , 392 ± 7.0 , and 393 ± 7.0 ppm in

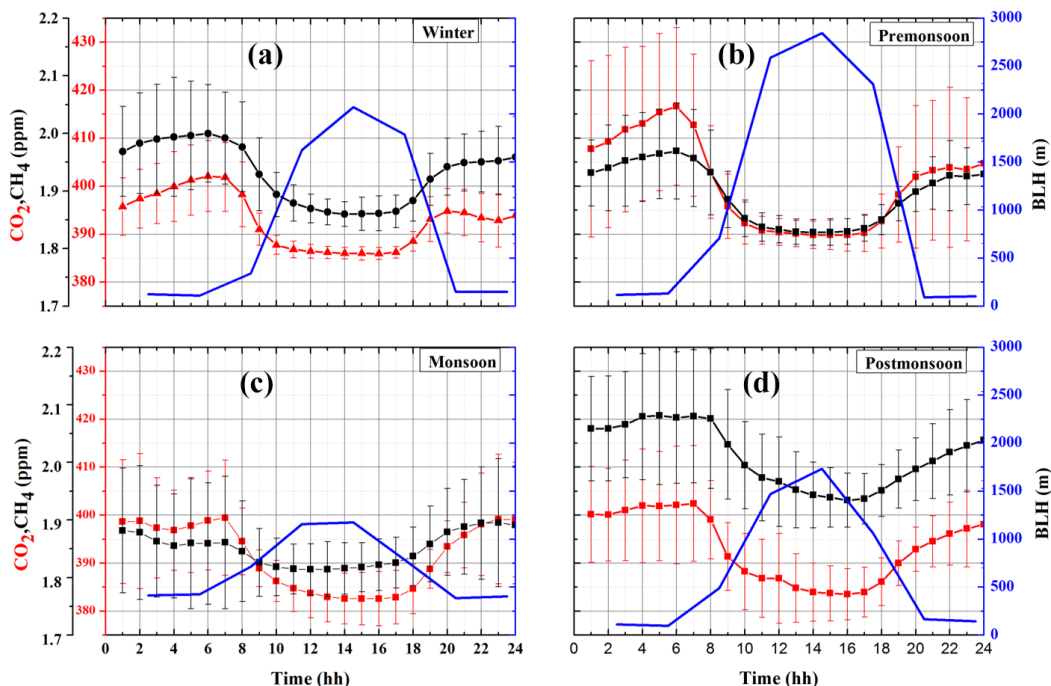


Figure 5. (a–d) Seasonal variations of diurnal averaged $\text{CO}_2 / \text{CH}_4$ against boundary layer height during 2014.

winter, pre-monsoon, monsoon, and post-monsoon respectively. Minimum CO_2 during winter (dry season) can be due to respiratory loss of carbon (Gilmanov et al., 2004; Aurela et al., 2004) as decreased temperature and solar radiation during this period inhibit increases in local CO_2 assimilation (Thum et al., 2009). A steady increase in CO_2 concentration is observed as season changes from winter to pre-monsoon months. Enhancement in pre-monsoon is due to higher temperature and solar radiation prevailing during these months, which stimulates the assimilation of CO_2 in the daytime and respiration in the night (Fang et al., 2014). The enhanced soil respiration during these months also complements the increase in CO_2 concentration during this period. In addition to these natural causes, biomass burning over the Indian region can also have a significant effect on pre-monsoon CO_2 concentration. A more detailed explanation of biomass burning influence on pre-monsoon GHG concentration over the study area is discussed in Sect. 4.2. Surface CO_2 concentration recorded a minimum during monsoon months mainly because of enhanced photosynthesis processes with the availability of greater soil moisture. A decrease in CO_2 concentration is also observed as the monsoon progresses. The decreases in temperature (due to cloudy and overcast conditions prevailing during these months) reduce leaf and soil respiration, which contributes to the enhancement of carbon uptake (Patil et al., 2013; Jing et al., 2010). Further increase during post-monsoon CO_2 is associated with high ecosystem productivity (Sharma et al., 2014) as well as an enhancement in soil microbial activity (Kirschke et al., 2013).

CH_4 concentration in the troposphere is principally determined by a balance between surface emission and destruction by OH. The major sources for CH_4 in the Indian region are rice, paddies, wetlands, and ruminants (Schneising et al., 2009). The annual CH_4 concentration over study area is observed to be 1.92 ± 0.07 ppm, with a maximum (2.02 ± 0.01 ppm) observed in post-monsoon and minimum (1.85 ± 0.03 ppm) in monsoon. Seasonal mean (average) values of CH_4 observed during different seasons are 1.93 ± 0.05 , 1.89 ± 0.05 , 1.85 ± 0.03 , and 2.02 ± 7 ppm in respectively winter, pre-monsoon, monsoon, and post-monsoon. The highest concentration appears during post-monsoon and may be associated with the Kharif season (Goroshiet al., 2011). Hayashida et al. (2013) reported that the seasonality of CH_4 concentration over monsoon Asia is characterized by higher values in the wet season and lower values in the dry season; possibly because of the effects of strong emissions from rice paddies and wetlands during the wet season. Low mixing ratios of CH_4 observed during monsoon season were mainly due to the reduction in atmospheric hydrocarbons because of the reduced photochemical reactions and the substantial reduction in solar intensity (Gaur et al., 2014). The rate of change of CH_4 was found to be high during post-monsoon. Both biological and physical processes control the exchange of CH_4 between rice paddy fields and the atmosphere (Nishanth et al., 2014; Goroshiet al., 2011). Due to this, enhanced CH_4 is observed during post-monsoon in the present study area.

4.2 Influence of vegetation on GHGs

In India, cropping season is classified into (i) Kharif and (ii) Rabi based on the onset of monsoon. The Kharif season is from July to October during the south-western monsoon and Rabi season is from October to March (Koshal, 2013). NDVI is one of the indicators of vegetation change, and monthly variations of CO₂ and CH₄ against NDVI are studied to understand the impact of land use and land cover on mixing ratios of CO₂ and CH₄. Monthly mean changes in NDVI, CO₂, and CH₄ are shown in Fig. 2c and d. Monthly mean of GHGs represented in this analysis is calculated from daily mean in daytime (10:00–16:00 LT). Analysis of the figure reveals that an inverse relationship exists between NDVI and CO₂, while a positive relation is observed w.r.t. CH₄. Generally over this part of the country vegetation starts during the month of June with the onset of south-western monsoon; as vegetation increases a decrease in CO₂ concentration is observed due to enhancement in photosynthesis. Further, a decline in NDVI is observed as the season advances from post-monsoon to winter and then to pre-monsoon, and it is associated with an increase in CO₂ concentration. Similarly, the main source for CH₄ emissions are soil microbial (Kirschke et al., 2013) activity which are more active during monsoon and post-monsoon seasons.

Biomass burning (forest fire and crop residue burning) is one of the major sources of gaseous pollutants such as carbon monoxide (CO₂), methane (CH₄), nitrous oxides (NO_x), and hydrocarbons in the troposphere (Crutzen et al., 1990, 1985; Sharma et al., 2010). In one of the recent studies, Jose et al. (2015a) analysed the atmospheric impact due to biomass mass burning over Hyderabad. In order to study the role of biomass burning on GHGs a case study is discussed. Figure 3c shows the spatial distribution of MODIS-derived fire counts over the Indian region during 14–21 April 2014 with air mass trajectories ending over study area overlaid on it at different altitudes, viz. 1000, 2000, and 4000 m respectively. Analysis of the figure shows a number of potential fire locations on the north-western and south-eastern side of study location and trajectories indicate its possible transport to study area. Daily mean variation of GHGs during the month of April 2014 (Fig. 3b) indicates an enhancement in GHGs during the same period (14–21 April 2014). Analysis reveals that CO₂ and CH₄ have increased by ~2 and ~0.06 % respectively during event days with respect to monthly mean. This analysis reveals that long-range/regional transported biomass burning have a role in enhancement of GHGs over study site. Further to understand the seasonal variation of biomass burning contribution to GHGs we analysed long-term (2003–2013) Fire Energetics and Emissions Research version 1.0 (FEER v1) data over study area. Emission coefficient (*C_e*) products during biomass burning are developed from coinciding measurements of fire radiative power and aerosol optical depth from MODIS Aqua and Terra satellites (Ichoku and Ellison, 2014). Figure 3a shows seasonal variation of

CO₂ emission due to biomass burning over the study site. Enhancement in CO₂ emission is seen during pre-monsoon months, which also supports earlier observation (Fig. 2a). This analysis reveals that biomass burning has a role in pre-monsoon enhancement of CO₂ over the study site. For a qualitative analysis of this long-range transport, we have analysed air mass trajectories ending over the study site during different seasons.

4.3 Correlation between CO₂ and CH₄

A correlation study is carried out between hourly averaged CO₂ and CH₄ during all season for the entire study period. The statistical analysis for different seasons is shown in Table 2. Fang et al. (2015) suggest the correlation coefficients (*R_s*) value higher than 0.50 indicates a similar source mechanism of CO₂ and CH₄. Also a positive correlation dominance of anthropogenic emission on carbon cycle. Our study also reveals a strong positive correlation observed between CO₂ and CH₄ during winter, pre-monsoon, monsoon, and post-monsoon with *R* equal to 0.80, 0.80, 0.61, and 0.72 respectively. The regression coefficients showed maximum (minimum) during winter and pre-monsoon (monsoon), which indicates the hourly stability of the mixing ratios between CO₂ and CH₄. This can be due to relatively simple source/sink processes of CO₂ in comparison to CH₄. Figure 4 shows the seasonal variation of $\Delta\text{CH}_4 / \Delta\text{CO}_2$. Dilution effects during transport of CH₄ and CO₂ can be minimized to some extent by dividing the increase of CH₄ over time by the respective increase in CO₂ (Worthy et al., 2009). In this study, background concentrations of respective GHGs are determined as mean values of the 1.25 percentile of data for monsoon, post-monsoon, pre-monsoon, and winter (Pan et al., 2011; Worthy et al., 2009). Annual $\Delta\text{CH}_4 / \Delta\text{CO}_2$ over the study region during the study period is found to be 7.1 (ppb ppm⁻¹). This low value clearly indicates the dominance of CO₂ over the study region. The reported $\Delta\text{CH}_4 / \Delta\text{CO}_2$ values from some of the rural sites, viz. Canadian Arctic and Hateruma Island (China), are of the order 12.2 and ~10 ppb ppm⁻¹ respectively (Worthy et al., 2009; Tohjima et al., 2014). Average $\Delta\text{CH}_4 / \Delta\text{CO}_2$ ratio during winter, pre-monsoon, monsoon, and post-monsoon are 9.40, 6.40, 4.40, and 8.20 ppb respectively. The monthly average of $\Delta\text{CH}_4 / \Delta\text{CO}_2$ is relatively high from late post-monsoon to winter, when the biotic activity is relatively dormant (Tohjima et al., 2014). During pre-monsoon the decrease in $\Delta\text{CH}_4 / \Delta\text{CO}_2$ ratio indicates the enhancement of CO₂ relative to that of CH₄.

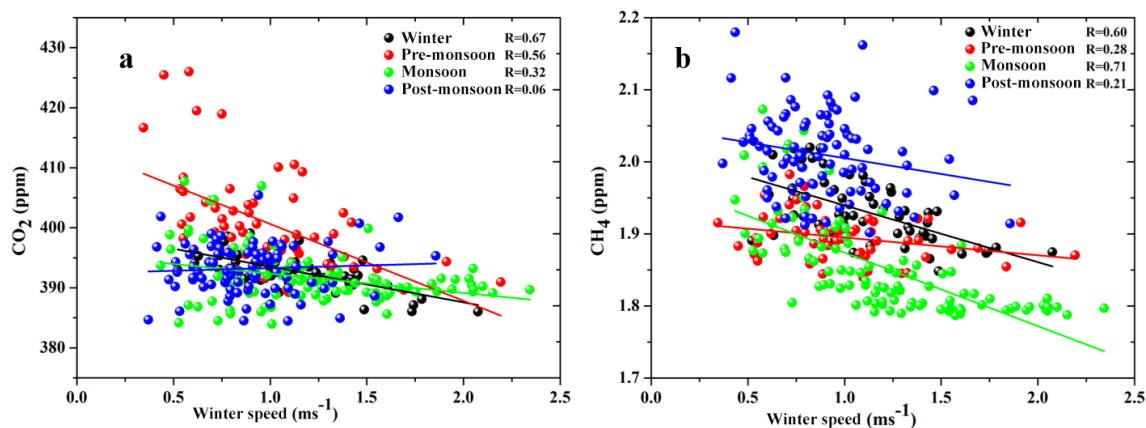


Figure 6. (a–b) Daily mean scatter plot of wind speed and GHGs (CO_2 and CH_4).

Table 3. Seasonal amplitudes of CO_2 and CH_4 over the study region arriving from different directions.

Wind direction	Winter CO_2 CH_4 (ppm)	Pre-monsoon CO_2 CH_4 (ppm)	Monsoon CO_2 CH_4 (ppm)	Post-monsoon CO_2 CH_4 (ppm)
0–45	399.85/1.98	410.37/1.94	400.72/1.91	395.13/2.02
45–90	391.66/1.94	399.59/1.89	388.82/1.91	390.23/1.98
90–135	391.57/1.93	397.79/1.87	388.99/1.87	389.06/1.97
135–180	389.34/1.89	393.87/1.85	391.81/1.86	387.69/1.97
180–225	391.14/1.89	396.75/1.85	390.28/1.82	392.30/2.02
225–270	389.13/1.88	394.81/1.86	390.26/1.82	384.40/1.94
270–315	388.68/1.87	398.68/1.89	389.58/1.82	384.99/1.93
315–360	390.87/1.91	401.17/1.89	387.58/1.83	389.32/1.98

4.4 Diurnal variations of CO_2 and CH_4

Figure 5a to d show the seasonally averaged diurnal cycle of CO_2 and CH_4 over Shadnagar during the study period. The vertical bar represents the standard deviation from the respective mean. Irrespective of seasonal variation, GHGs showed a similar diurnal variation, with maximum mixing ratios observed during early morning (6 h) as well as early night hours (20 h) and minimum during afternoon hours. However, the difference observed in the maximum diurnal amplitudes can be attributed to seasonal changes. The observed diurnal cycle of GHGs is closely associated with diurnal variation of the planetary boundary layer height. For better understanding of the diurnal behaviour of CO_2 / CH_4 , we used European Centre for Medium-range Weather Forecasting (ECMWF) Interim Reanalysis (ERA) PBL data set, which gives data for every 3 h, viz. 00:00, 03:00, 06:00, 09:00, 12:00, 15:00, 18:00, and 21:00 UTC with a resolution of $0.25^\circ \times 0.25^\circ$ (<http://data-portal.ecmwf.int>). Figure 5a to d portray the diurnal evolution of CO_2 / CH_4 during different seasons along with the evolution of BLH (m) on the secondary y axis. The morning peak arises due to combined influence of the fumigation effect (Stull 1988) and morning build-up of local anthropogenic activities (household and ve-

hicular transport). The low value of GHGs as the day progresses can be attributed to increased photosynthetic activity during daytime and the destruction of stable boundary layer and residual layer due to convective activity. In the evening hours, surface inversion begins and form a shallow stable boundary layer, causing the enhancement in GHG concentration near the surface. A similar trend in diurnal variation of GHGs is reported from other parts of the country (Patil et al., 2013; Mahesh et al., 2013; Sharma et al., 2014; Nishanth et al., 2014).

4.5 Influence of prevailing meteorology

Redistribution (both horizontal and vertical) of GHGs also plays a role in their seasonal variation, as it controls transport and diffusion of pollutants from one place to another (Hasan, 2015). A good inverse correlation between wind speed and GHGs suggests the proximity of sources near the measurement site, while a not so significant correlation suggests the influence of regional transport (Ramachandran and Ramesh, 2007). Figure 6a and b show a scatter plot of the GHGs and wind speed during different seasons. Analysis of Fig. 6 shows that an inverse correlation exists between daily mean wind speed and GHGs. Correlation coefficients (R_s) between

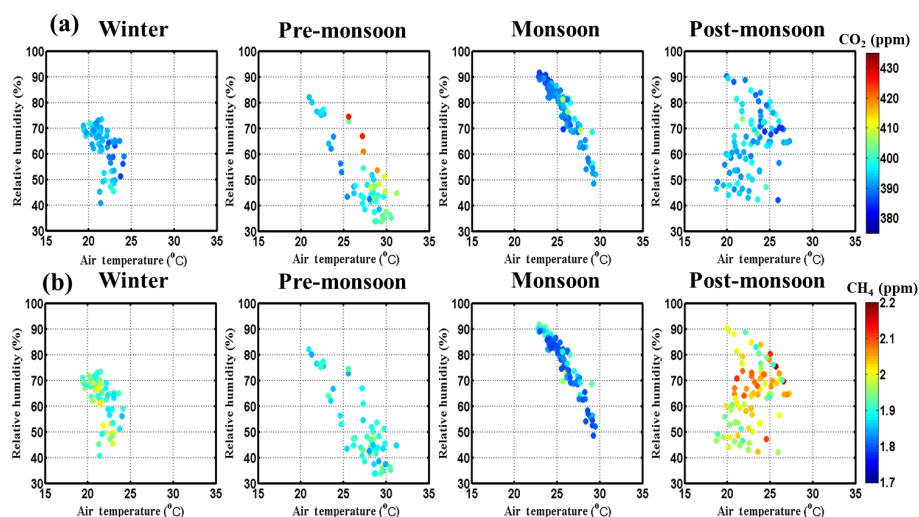


Figure 7. (a–b) Daily means seasonal variation of CO_2 and CH_4 as a function of humidity and air temperature during 2014.

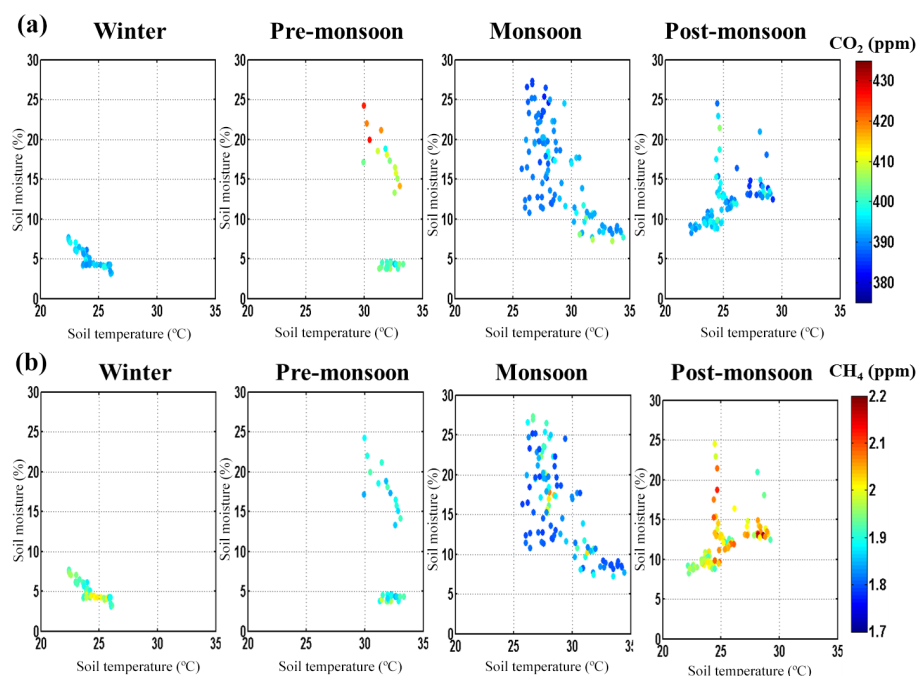


Figure 8. (a–b) Daily means seasonal variation of CO_2 and CH_4 as a function of soil temperature and soil moisture during 2014.

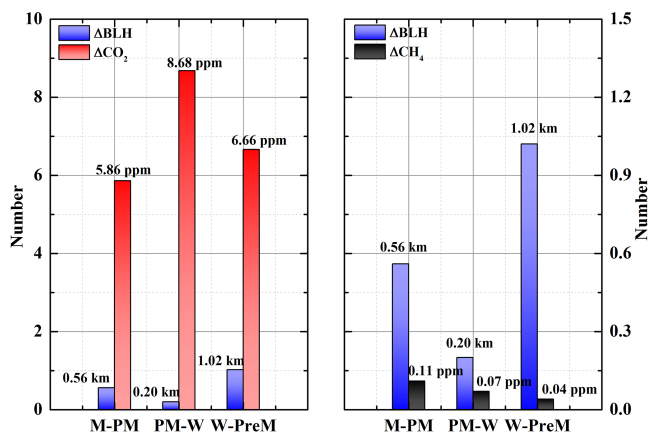
wind speed and CO_2 during pre-monsoon, monsoon, post-monsoon, and winter are 0.56, 0.32, 0.06, and 0.67 respectively, while for CH_4 they are found to be 0.28, 0.71, 0.21, and 0.60 respectively. The negative correlation indicates that the influence of local sources on GHGs; however, the poor correlation coefficients during different seasons suggest the role of regional/local transport (Mahesh et al., 2014). Also, an understanding of prevailing wind direction and its relationship with GHGs helps in determining their probable source regions. Table 3 shows the monthly mean variation of CO_2 and CH_4 with respect to different wind directions. Enhancements

in the CO_2 and CH_4 levels over Shadnagar are observed to mainly come from north-west and north-east, while the lowest are from the south and south-west. This can be associated to some extent with industrial emissions located on the western side of the sampling site and the influence of emission and transport from the nearby urban centre on the north-western side of the study site.

The influence of meteorological parameters (temperature and relative humidity) on trace gases is also examined. Figure 7a and b (top panel corresponds to CO_2 and bottom panel represents CH_4) show the scatter plot of temperature vs. rel-

Table 4. Cluster analysis of air mass trajectories reaching Shadnagar at various heights during different seasons.

Seasonal Backward trajectory (%)	NW				NE				SE				SW			
	1 km	2 km	3 km	4 km	1 km	2 km	3 km	4 km	1 km	2 km	3 km	4 km	1 km	2 km	3 km	4 km
Winter	54	32	2	0	32	24	44	52	10	25	11	7	4	19	42	41
Pre-monsoon	24	9	8	1	26	31	64	78	36	46	2	10	14	14	26	11
Monsoon	0	1	7	19	12	34	80	70	4	4	4	6	84	61	9	5
Post-monsoon	42	15	11	14	47	53	41	49	8	30	32	26	3	2	16	11

**Figure 9.** Seasonal differences in BLH against respective change in (a) CO₂ and (b) CH₄.

ative humidity as a function of GHGs during different seasons. Daily mean data are used instead of hourly mean data to avoid the influence of the diurnal variations on correlations. CO₂ showed a positive correlation with temperature during all seasons except winter. This negative correlation can be attributed to different responses of the photosynthesis rate to different air temperature. IPCC (1990) reports that many mid-latitude plants show an optimum gross photosynthesis rate when temperature varied from 20 to 35 °C. The rate of plant respiration tends to be slow below 20 °C. However, at higher temperatures, the respiration rate accelerates rapidly up to a temperature at which it equals the rate of gross photosynthesis and there can be no net assimilation of carbon. While CH₄ showed a weak positive correlation with temperature during pre-monsoon and post-monsoon, a weak negative correlation is observed during monsoon and winter. This could be due to the rate of chemical loss reaction with OH being faster in summer and slower in other seasons. A case study on CH₄ sink mechanism is discussed in Sect. 4.6. Seasonal variation of GHGs also showed an insignificantly negative correlation with RH. One of the supporting arguments is that in humid conditions these stoma can fully open to increase the uptake of CO₂ without a net water loss. Also, wetter soils can promote decomposition of dead plant mate-

rials, releasing natural fertilizers that help plants grow (Gaur et al., 2014).

Figure 8a and b illustrate the daily mean variation of GHGs with respect to soil moisture and soil temperature (top panel represents the seasonal variation of CO₂ w.r.t. soil moisture and soil temperature, while the bottom panel represents the seasonal variation of CH₄ against the same parameters). It is quite interesting to observe that GHGs behave differently w.r.t. soil moisture during different seasons. CH₄ shows a positive relationship during monsoon and post-monsoon and an inverse relationship during pre-monsoon and winter, while a reverse relationship exists for CO₂. During the wet season aeration is restricted (Smith et al., 2003); hence soil respiration is limited, which decrease CO₂ flux. This may be one of the factors leading to low values of CO₂ during monsoon months; during dry months soil may act as a sink of CH.

Influence of BLH on GHG mixing ratios

The PBL is the lowest layer of the troposphere, where wind speed as a function of temperature plays a major role in its thickness variation. It is an important parameter for controlling the observed diurnal variations and potentially masking the emissions signal (Newman et al., 2013). Since a complete set of COSMIC-RO data is not available during the study period, in this analysis we have analysed RO data from July 2013 to June 2014, along with simultaneous observations of GHGs. Monthly variations (figure not show) of BLH are computed from high-vertical-resolution COSMIC-RO data and compared against CO₂ and CH₄ concentrations. Monthly BLH is observed to be minimum (maximum) during winter and monsoon (pre-monsoon) seasons and it closely resembles with the air temperature pattern. The highest (lowest) BLH over the study region was identified as 3.20 km (1.50 km). The monthly average air temperature was at maximum (minimum) 29 °C (20 °C) during the summer (winter) months.

Seasonal BLHs during winter, pre-monsoon, monsoon, and post-monsoon are 2.10, 3.15, 1.74, and 2.30 km respectively. The influence of BLH on CO₂ and CH₄ mixing ratios is shown in Fig. 9a and b. The *x* axis represents the seasonal transition, i.e. monsoon to post-monsoon, and the *y* axis indicates seasonal difference of BLH and GHG concentrations.

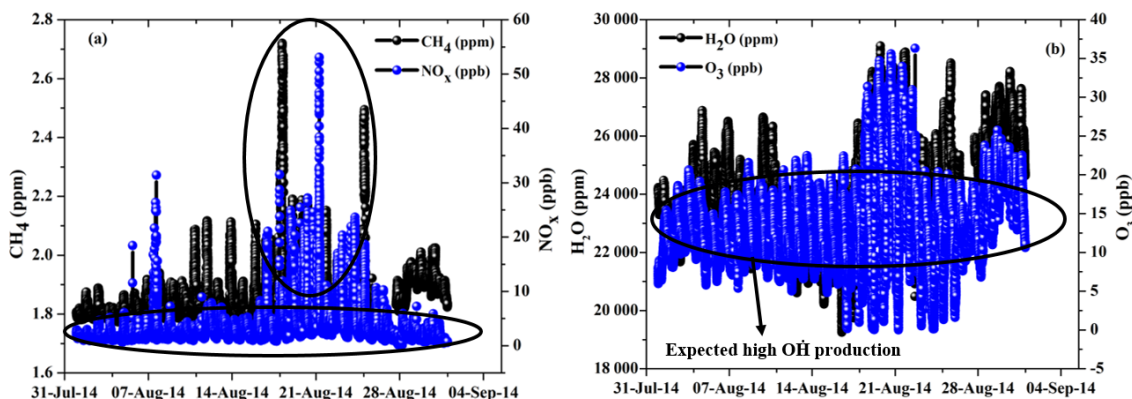


Figure 10. Time series analysis of (a) CH_4 vs. NO_x and (b) H_2O vs. O_3 .

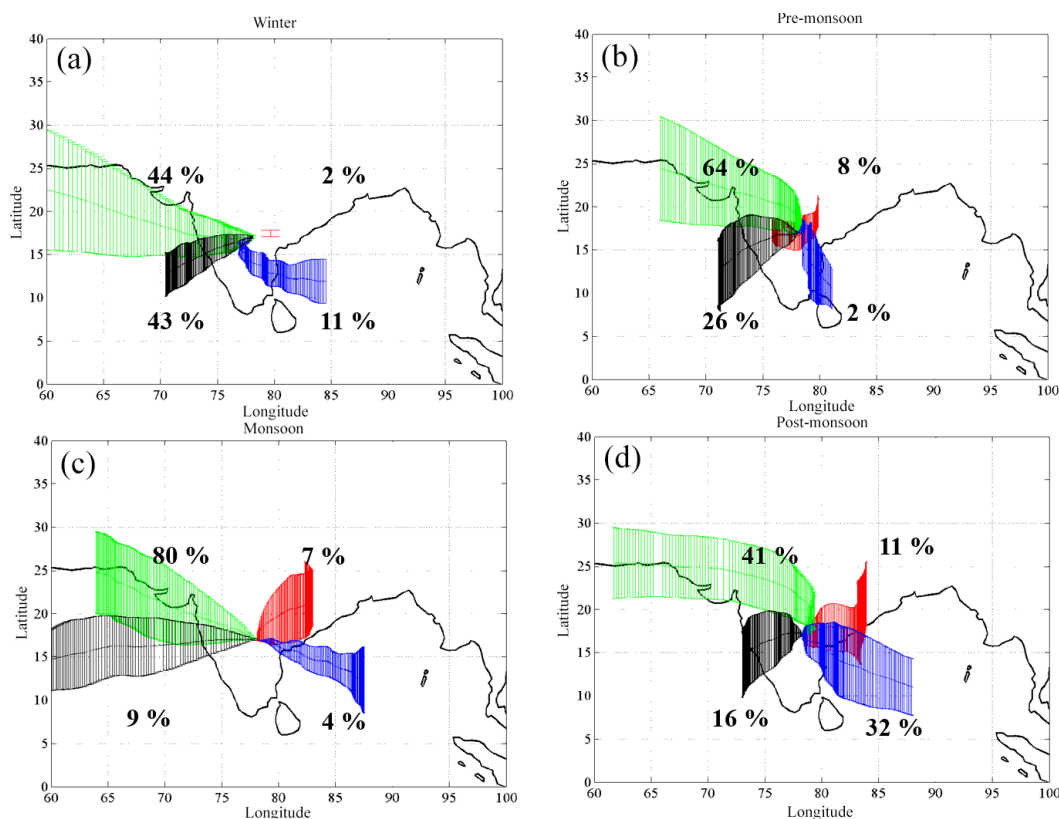


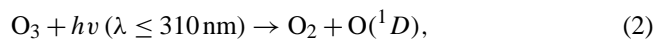
Figure 11. (a–d) Long-range circulation of air mass trajectories ending over Shadnagar at 3 km during winter, pre-monsoon, monsoon, and post-monsoon.

As seasonal BLHs increase, mixing ratios of CO_2 (CH_4) decrease from 8.68 to 5.86 ppm (110 to 40 ppb). This effect was clearly captured by seasonal diurnal averaged BLH data sets used from ECMWF-ERA. The influence of biosphere emissions on CO_2 and CH_4 can be estimated through atmospheric boundary layer processes. Since the study region is a flat terrain, variations in CO_2 and CH_4 were mostly influenced by BLH through convection and biosphere activities.

4.6 Methane (CH_4) sink mechanism

Methane (CH_4) is the most powerful greenhouse gas in the atmosphere after CO_2 due to its strong positive radiative forcing (Stocker et al., 2013). Atmospheric CH_4 is mainly (70–80 %) of biological origin, produced in anoxic environments by anaerobic digestion of organic matter (Crutzen and Zimmermann, 1991). The major CH_4 sink is oxidation by OH, which account for 90 % of CH_4 sink (Vaghjiani and Ravis-

hankara, 1991; Kim et al., 2015). OH radicals are very reactive and are responsible for the oxidation of almost all gases in the atmosphere. The primary source for OH radical formation in the atmosphere is photolysis of ozone (O_3) and water vapour (H_2O). Eisele et al. (1997) defined primary and secondary sources of OH radicals in the atmosphere. The primary source of OH radical is as follows:



where $O(^1D)$ is the electronically excited atom.



Removal of CH_4 is constrained by the presence of OH radicals in the atmosphere. A 1 min time series analysis of CH_4 , NO_x , O_3 , and H_2O and associated wind vector for August 2014 is shown in Fig. 10a and b to understand the CH_4 chemistry. Low NO_x (1–2 ppb) values are shown in horizontal elliptical region of Fig. 10a and observed corresponding low CH_4 (1.80 ppm) concentrations. The low NO_x in turn produces high OH radicals in the atmosphere due to conversion of HO_2 radical by NO, which removes CH_4 through oxidation process as shown below.



when NO_x levels are 1–2 ppb. The main CH_4 removal process is



if $NO_x > 2$ ppb ($OH \downarrow$, $CH_4 \uparrow$). Crutzen and Zimmermann (1991) and Eisele et al. (1997) observed that at low NO_x (0.5–2.0 ppb) levels most HO_x family radicals such as HO_2 and peroxy radicals (RO_2) react with NO to form OH radicals. Therefore OH radicals are much higher in the case of low NO_x . When NO_x levels increase more than 2 ppb, most of the OH radicals react with NO_2 to form nitric acid (HNO_3). In first order, the levels of CH_4 in the atmosphere depend on the levels of NO_x though the production of OH radicals in the atmosphere is still uncertain. Figure 10a and b show high CH_4 , H_2O , O_3 , and NO_x over a few days in August 2014. High concentrations of CH_4 , NO_x , and other gases are observed in the eastern direction of study site. Very high NO_x levels above 10 ppb are observed, and subsequently CH_4 concentrations also increased to 2.40 ppm from 1.80 ppm. In the eastern direction of study site a national highway and single line broad gauge railway network are present, which act as possible sources of NO_x , CH_4 , and CO_2 . An increase in emissions of NO_x causes a decline in the levels of OH radicals and subsequently observed high CH_4 over the study region.

4.7 Long-range circulations

To understand the role of long-range circulation, we separated the trajectory into four clusters based on their pathway, namely north-east, north-west, south-east, and south-west. The main criterion of trajectory clustering is to minimize the variability among trajectories and maximize variability among clusters. Cluster mean trajectories of air mass (Jose et al., 2015b) and their percentage contribution to the total calculated for each season over the study period at 3 km altitude are depicted in Fig. 11. The majority of air mass trajectories during winter ($\sim 44\%$), pre-monsoon ($\sim 64\%$), monsoon ($\sim 80\%$), and post-monsoon ($\sim 41\%$) originate from north-western parts of the study site. For a comprehensive analysis, percentage occurrences of cluster mean trajectories of air mass over study area during different seasons at different altitudes are also tabulated in Table 4. Agriculture residue burning is commonly observed in the NW and NE regions of India during the post-harvest period extending from the post-monsoon period to the pre-monsoon period (Sharma et al., 2010). Our analysis reveals that during this period, the majority of air mass reaching the study site at different altitudes comes from this part of the country.

5 Conclusions

The present study analysed the seasonal variations of atmospheric GHGs (CO_2 and CH_4) and associated prevailing meteorology over Shadnagar, a suburban site of Central India, during the period 2014. The salient findings of the study are the following.

- Irrespective of seasons, major sources for CO_2 are soil respiration and anthropogenic emissions while vegetation acts as a main sink, whereas the major source and sink for CH_4 are vegetation and the presence of OH radicals. In addition, boundary layer dynamics and long-range transport also play a vital role in GHG mixing ratios.
- The annual means of CO_2 and CH_4 over the study region are found to be 394 ± 2.92 and 1.92 ± 0.07 ppm ($\mu \pm 1\sigma$) respectively. CO_2 and CH_4 show a significant seasonal variation during the study period. Maximum (minimum) CO_2 is observed during pre-monsoon (monsoon), while CH_4 recorded maximum during post-monsoon and minimum during monsoon. Seasonal analysis of FEER data also showed maximum emission of CO_2 due to biomass burning during pre-monsoon months, which indicates the influence of biomass burning on local emissions.
- CO_2 and CH_4 showed consistent diurnal behaviour in spite of their significant seasonal variations, with an observed morning (06:00 IST) maxima, followed by af-

ternoon minima (14:00 IST) and enhancing in the late evening (~ 22:00 IST).

- Correlation coefficients (R_s) between wind speed and CO₂ during pre-monsoon, monsoon, post-monsoon, and winter are 0.56, 0.32, 0.06, and 0.67 respectively, while for CH₄ they are found to be 0.28, 0.71, 0.21, and 0.60 respectively. The negative correlation indicates that the influence of local sources on GHGs; however, poor correlation coefficients during different seasons suggest the role of regional/local transport.
- CO₂ showed a positive correlation with temperature during all seasons except winter. CH₄ showed a weak positive correlation with temperature during pre-monsoon and post-monsoon while showing a weak negative correlation during monsoon and winter.
- CO₂ and CH₄ showed a strong positive correlation during winter, pre-monsoon, monsoon, and post-monsoon with R_s equal to 0.80, 0.80, 0.61, and 0.72 respectively. This clearly indicates common anthropogenic sources for these gases.

Acknowledgement. This work was part of the Atmospheric CO₂ Retrieval and Monitoring (ACRM) under National Carbon Project (NCP) of ISRO-GBP. The authors sincerely acknowledge Biswadip Gharai, ACSG/ECSA, for providing LULC data and to K. Mallikarjun, ACSG/ECSA, for his support in data collection. We thank Data and Product Quality Evaluation (D & PQE), division of NRSC, and P. Sujatha, ACSG, for sharing AWS and boundary layer data. The authors are grateful to the AT-CTM project of ISRO-GBP for providing the O₃ and NO_x analyzers. We would also like to thank the HYSPLIT, ECMWF-ERA, MODIS, and COSMIC teams for providing the scientific data sets used in this study. We also thank the anonymous referees and the editor for providing constructive suggestions which certainly improved the quality of the manuscript.

Edited by: J. Huang

References

- Ao, C. O., Waliser, D. E., Chan, S. K., Li, J.-L., Tian, B., Xie, F., and Mannucci, A. J.: Planetary boundary layer heights from GPS radio occultation refractivity and humidity profiles, *J. Geophys. Res.*, 117, D16117, doi:10.1029/2012JD017598, 2012.
- Aurela, M., Lohila, A., Tuovinen, J. P., Hatakka, J., Riutta, T., and Laurila, T.: Carbon dioxide exchange on a northern boreal fen, *Boreal Environ. Res.*, 14, 699–710, 2009.
- Baer, D. S., Paul, J. B., Gupta, M., and O’Keefe, A.: Sensitive absorption measurements in the near-infrared region using off-axis integrated-cavity-output spectroscopy, *Appl. Phys. B*, 75, 261–265, 2002.
- Berman, E. S., Fladland, M., Liem, J., Kolyer, R., and Gupta, M.: Greenhouse gas analyzer for measurements of carbon dioxide, methane, and water vapor aboard an unmanned aerial vehicle, *Sensors and Actua. B-Chem.*, 169, 128–135, 2012.
- Crutzen, P. J.: Methane’s sinks and sources, *Nature*, 350, 380–381, 1991.
- Crutzen, P. J. and Andreae, M. O.: Biomass burning in the tropics: Impact on atmospheric chemistry and biogeochemical cycles, *Science*, 250, 1669–1678, 1990.
- Crutzen, P. J. and Zimmermann, P. H.: The changing photochemistry of the troposphere, *Tellus B*, 43, 136–151, 1991.
- Crutzen, P. J., Delany, A. C., Greenberg, J., Haagenson, P., Heidt, L., Lueb, R., Pollock, W., Wartburg, S., Wartburg, A., and Zimmermann, P.: Tropospheric chemical composition measurements in Brazil during the dry season, *J. Atmos. Chem.*, 2, 233–256, 1985.
- Draxler, R. R. and Rolph, G. D.: HYSPLIT (Hybrid Single Particle Lagrangian Integrated Trajectory) Model access via NOAA ARL READY website (<http://www.arl.noaa.gov/ready/hysplit4.html>), NOAA Air Resources Laboratory, Silver Spring, MD, 2003.
- Eisele, F. L., Mount, G. H., Tanner, D., Jefferson, A., Shetter, R., Harder, J. W., and Williams, E. J.: Understanding the production and interconversion of the hydroxyl radical during the Tropospheric OH Photochemistry Experiment, *J. Geophys. Res.-Atmos.*, 102, 6457–6465, 1997.
- Fang, S. X., Zhou, L. X., Tans, P. P., Ciais, P., Steinbacher, M., Xu, L., and Luan, T.: In situ measurement of atmospheric CO₂ at the four WMO/GAW stations in China, *Atmos. Chem. Phys.*, 14, 2541–2554, doi:10.5194/acp-14-2541-2014, 2014.
- Fang, S. X., Tans, P. P., Steinbacher, M., Zhou, L. X., and Luan, T.: Comparison of the regional CO₂ mole fraction filtering approaches at a WMO/GAW regional station in China, *Atmos. Meas. Tech.*, 8, 5301–5313, doi:10.5194/amt-8-5301-2015, 2015.
- Frankenberg, C., Bergamaschi, P., Butz, A., Houweling, S., Fokke Meirink, J., J. Notholt, Petersen, A. K., Schrijver, H., Warneke, T., and Aben, I.: Tropical methane emissions: A revised view from SCIAMACHY onboard ENVISAT, *Geophys. Res. Lett.*, 35, 15, doi:10.1029/2008GL034300, 2008.
- Garg, A., Bhattacharya, S., Shukla, P. R., and Dadhwal, V. K.: Regional and sectoral assessment of greenhouse gas emissions in India, *Atmos. Environ.*, 35, 2679–2695, 2001.
- Gaur, A., Tripathi, S. N., Kanawade, V. P., Tare, V., and Shukla, S. P.: Four-year measurements of trace gases (SO₂, NO_x, CO, and O₃) at an urban location, Kanpur, in Northern India, *J. Atmos. Chem.*, 71, 283–301, 2014.
- Gilmanov, T. G., Johnson, D. A., Saliendra, N. Z., Akshalov, K., and Wylie, B. K.: Gross primary productivity of the true steppe in Central Asia in relation to NDVI: scaling up CO₂ fluxes, *Environ. Manage.*, 33, S492–S508, 2004.
- Goroshi, S. K., Singh, R. P., Panigrahy, S., and Parihar, J. S.: Analysis of seasonal variability of vegetation and methane concentration over India using SPOT-VEGETATION and ENVISAT-SCIAMACHY data, *J. Indian Soc. Remote Sens.*, 39, 315–321, 2011.
- Hassan, A. G. A.: Diurnal and Monthly Variations in Atmospheric CO₂ Level in Qena, Upper Egypt, *Resour. Environ.*, 5, 59–65, 2015.

- Hayashida, S., Ono, A., Yoshizaki, S., Frankenberg, C., Takeuchi, W., and Yan, X.: Methane concentrations over Monsoon Asia as observed by SCIAMACHY: Signals of methane emission from rice cultivation, *Remote Sens. Environ.*, 139, 246–256, 2013.
- Huang, J. P., Zhang, W., Zuo, J. Q., Bi, J. R., Shi, J. S., Wang, X., Chang, Z. L., Huang, Z. W., Yang, S., Zhang, B. D., Wang, G. Y., Feng, G. H., Yuan, J. Y., Zhang, L., Zuo, H. C., Wang, S. G., Fu, C. B., and Chou, J. F.: An overview of the semi-arid climate and environment research observatory over the Loess Plateau, *Adv. Atmos. Sci.*, 25, 906–921, 2008.
- Huang, J., Yu, H., Guan, X., Wang, G., and Guo, R.: Accelerated dryland expansion under climate change, *Nature Climate Change*, 6, 166–171, 2015.
- Ichoku, C. and Ellison, L.: Global top-down smoke-aerosol emissions estimation using satellite fire radiative power measurements, *Atmos. Chem. Phys.*, 14, 6643–6667, doi:10.5194/acp-14-6643-2014, 2014.
- Intergovernmental Panel on Climate Change (IPCC): *Climate Change: The IPCC Scientific Assessment*, edited by: Houghton, J. T., Jerkins, G. J., and Ephraums, J. J., Cambridge University Press, New York, 1990.
- James, M. E. and Kalluri, S. N.: The Pathfinder AVHRR land data set: an improved coarse resolution data set for terrestrial monitoring, *Int. J. Remote Sens.*, 15, 3347–3363, 1994.
- Jing, X., Huang, J., Wang, G., Higuchi, K., Bi, J., Sun, Y., and Wang, T.: The effects of clouds and aerosols on net ecosystem CO₂ exchange over semi-arid Loess Plateau of Northwest China, *Atmos. Chem. Phys.*, 10, 8205–8218, doi:10.5194/acp-10-8205-2010, 2010.
- Jones, C., McConnell, C., Coleman, K., Cox, P., Falloon, P., Jenkinson, D., and Powlson, D.: Global climate change and soil carbon stocks; predictions from two contrasting models for the turnover of organic carbon in soil, *Glob. Change Biol.*, 11, 154–166, 2005.
- Jose, S., Gharai, B., Kumar, Y. B., and Rao, P. V. N.: Radiative implication of a haze event over Eastern India, *Atmos. Pollut. Res.*, 6, 138–146, 2015a.
- Jose, S., Niranjana, K., Gharai, B., and Rao, P. V. N.: Characterisation of absorbing aerosols using ground and satellite data at an urban location, Hyderabad, *Aerosol Air Qual. Res.*, in press, doi:10.4209/aaqr.2014.09.0220, 2015b.
- Keppler, F., Hamilton, J. T., Braß, M., and Röckmann, T.: Methane emissions from terrestrial plants under aerobic conditions, *Nature*, 439, 187–191, 2006.
- Kim, H. S., Chung, Y. S., Tans, P. P., and Dlugokencky, E. J.: Decadal trends of atmospheric methane in East Asia from 1991 to 2013, *Air Qual. Atmos. Health*, 8, 293–298, 2015.
- King, M. D., Kaufman, Y. J., Menzel, W. P., and Tanre, D.: Remote sensing of cloud, aerosol, and water vapor properties from the Moderate Resolution Imaging Spectrometer (MODIS), *Geosci. Remote Sens.*, 30, 2–27, 1992.
- Kirschke, S., Bousquet, P., Ciais, P., Saunoy, M., Canadell, J. G., Dlugokencky, E. J., Bergamaschi, P., Bergmann, D., Blake, D. R., Bruhwiler, L., Cameron-Smith, P., Castaldi, S., Chevallier, F., Feng, L., Fraser, A., Heimann, M., Hodson, E. L., Houweling, S., Josse, B., Fraser, P. J., Krummel, P. B., Lamarque, J.-F., Langenfelds, R. L., Le Quééré, C., Naik, V., O'Doherty, S., Palmer, P. I., Pison, I., Plummer, D., Poulter, B., Prinn, R. G., Rigby, M., Ringeval, B., Santini, M., Schmidt, M., Shindell, D. T., Simpson, I. J., Spahni, R., Steele, L. P., Strode, S. A., Sudo, K., Szopa, S., van der Werf, G. R., Voulgarakis, A., Weele, M., Weiss, R. F., Williams, J. E., and Guang, Z.: Three decades of global methane sources and sinks, *Nature Geosci.*, 6, 813–823, 2013.
- Koshal, A. K.: Spatial temporal climatic change variability of cropping system in western Uttar Pradesh, *Int. J. Remote Sens. Geosci.*, 2, 36–45, 2013.
- Liu, Y., Wang, X., Guo, M., Tani, H., Matsuoka, N., and Matsumura, S.: Spatial and temporal relationships among NDVI, climate factors, and land cover changes in Northeast Asia from 1982 to 2009, *GI, Sci. Remote Sens.*, 48, 371–393, 2011.
- Machida, T., Kita, K., Kondo, Y., Blake, D., Kawakami, S., Inoue, G., and Ogawa, T.: Vertical and meridional distributions of the atmospheric CO₂ mixing ratio between northern mid-latitudes and southern subtropics, *J. Geophys. Res.*, 107, 8401, doi:10.1029/2001JD000910, 2002.
- Mahesh, P., Sharma, N., Dadhwal, V. K., Rao, P. V. N., and Apparao, B. V.: Impact of Land-Sea Breeze and Rainfall on CO₂ Variations at a Coastal Station, *J. Earth Sci. Clim. Change*, 5, 201, doi:10.4172/2157-7617.1000201, 2014.
- Mahesh, P., Sreenivas, G., Rao, P. V. N., Dadhwal, V. K., Sai Krishna, S. V. S., and Mallikarjun, K.: High precision surface level CO₂ and CH₄ using Off-Axis Integrated Cavity Output Spectroscopy (OA-ICOS) over Shadnagar, India, *Int. J. Remote Sens.*, 36, 5754–5765, doi:10.1080/01431161.2015.1104744, 2015.
- Miller, J. B., Gatti, L. V., d'Amelio, M. T. S., Crotwell, A. M., Dlugokencky, E. J., Bakwin, P., Artaxo, P., and Tans, P. P.: Airborne measurements indicate large methane emissions from the eastern Amazon basin, *Geophys. Res. Lett.*, 34, L10809, doi:10.1029/2006GL029213, 2007.
- Monastersky, R.: Global carbon dioxide levels near worrisome milestone, *Nature*, 497, 7447, doi:10.1038/497013a, 2013.
- Newman, S., Jeong, S., Fischer, M. L., Xu, X., Haman, C. L., Lefler, B., Alvarez, S., Rappenglueck, B., Kort, E. A., Andrews, A. E., Peischl, J., Gurney, K. R., Miller, C. E., and Yung, Y. L.: Diurnal tracking of anthropogenic CO₂ emissions in the Los Angeles basin megacity during spring, *Atmos. Chem. Phys.*, 13, 4359–4372, doi:10.5194/acp-13-4359-2013, 2013.
- Nishanth, T., Praseed, K. M., Satheesh, Kumar M. K., and Valsaraj, K. T.: Observational study of surface O₃, NO_x, CH₄ and total NMHCs at Kannur, India, *Aerosol. Air. Qual. Res.*, 14, 1074–1088, 2014.
- Pan, X. L., Kanaya, Y., Wang, Z. F., Liu, Y., Pochanart, P., Akiyama, H., Sun, Y. L., Dong, H. B., Li, J., Irie, H., and Takigawa, M.: Correlation of black carbon aerosol and carbon monoxide in the high-altitude environment of Mt. Huang in Eastern China, *Atmos. Chem. Phys.*, 11, 9735–9747, doi:10.5194/acp-11-9735-2011, 2011.
- Paul, J. B., Lapson, L., and Anderson, J. G.: Ultrasensitive absorption spectroscopy with a high-finesse optical cavity and off-axis alignment, *Appl. Optics*, 40, 4904–4910, 2001.
- Patil, M. N., Dharmaraj, T., Waghmare, R. T., Prabha, T. V., and Kulkarni, J. R.: Measurements of carbon dioxide and heat fluxes during monsoon-2011 season over rural site of India by eddy covariance technique, *J. Earth Syst. Sci.*, 123, 177–185, 2014.
- Pielke, R. A., Marland, G., Betts, R. A., Chase, T. N., Eastman, J. L., Niles, J. O., and Running, S. W.: The influence of land-use change and landscape dynamics on the climate system: relevance to climate-change policy beyond the radiative effect of greenhouse gases, *Philos. Tr. R. Soc. Lon.*, 360, 1705–1719, 2002.

- Ramachandran, S. and Rajesh, T. A.: Black carbon aerosol mass concentrations over Ahmedabad, an urban location in western India: comparison with urban sites in Asia, Europe, Canada, and the United States, *J. Geophys. Res.-Atmos.*, 112, D06211, doi:10.1029/2006JD007488, 2007.
- Salomonson, V. V., Barnes, W. L., Maymon, P. W., Montgomery, H. E., and Ostrow, H.: MODIS: Advanced facility instrument for studies of the Earth as a system, *Geosci. Remote Sens.*, 27, 145–153, 1989.
- Smith, K. A., Ball, T., Conen, F., Dobbie, K. E., Massheder, J., and Rey, A.: Exchange of greenhouse gases between soil and atmosphere: interactions of soil physical factors and biological processes, *Eur. J. Soil Sci.*, 54, 779–791, 2003.
- Schneising, O., Buchwitz, M., Burrows, J. P., Bovensmann, H., Bergamaschi, P., and Peters, W.: Three years of greenhouse gas column-averaged dry air mole fractions retrieved from satellite – Part 2: Methane, *Atmos. Chem. Phys.* 9, 443–465, doi:10.5194/acp-9-443-2009, 2009.
- Sharma, A. R., Kumar Kharol, S., Badarinath, K. V. S., and Singh, D.: Impact of agriculture crop residue burning on atmospheric aerosol loading – a study over Punjab State, India, www.ann-geophys.net/28/367/2010/, *Ann. Geophys.*, 28, p. 367, 2010.
- Sharma, N., Dadhwal, V. K., Kant, Y., Mahesh, P., Mallikarjun, K., Gadavi, H., Sharma, A., and Ali, M. M.: Atmospheric CO₂ Variations in Two Contrasting Environmental Sites Over India, *Air Soil Water Res.*, 7, 61–68, 2014.
- Sharma, N., Nayak, R. K., Dadhwal, V. K., Kant, Y., and Ali, M. M.: Temporal variations of atmospheric CO₂ in Dehradun, India during 2009, *Air Soil Water Res.*, 6, 37–45, doi:10.4137/ASWR.S10590, 2013.
- Shea, S. J. O., Allen, G., Gallagher, M. W., Bauguitte, S. J.-B., Illingworth, S. M., Le Breton, M., Muller, J. B. A., Percival, C. J., Archibald, A. T., Oram, D. E., Parrington, M., Palmer, P. I., and Lewis, A. C.: Airborne observations of trace gases over boreal Canada during BORTAS: campaign climatology, air mass analysis and enhancement ratios., *Atmos. Chem. Phys.*, 13, 12451–12467, doi:10.5194/acp-13-12451-2013, 2013.
- Stocker, T. F., Qin, D., Plattner, G. K., Alexander, L. V., Allen, S. K., Bindoff, N. L., Bréon, F. M., Church, J. A., Cubasch, U., Emori, S., Forster, P., Friedlingstein, P., Gillett, N., Gregory, J. M., Hartmann, D. L., Jansen, E., Kirtman, B., Knutti, R., Krishna Kumar, K., Lemke, P., Marotzke, J., Masson-Delmotte, V., Meehl, G. A., Mokhov, I. I., Piao, S., Ramaswamy, V., Randall, D., Rhein, M., Rojas, M., Sabine, C., Shindell, D., Talley, L. D., Vaughan D. G., and Xie, S. P.: Technical Summary, in: *Climate Change 2013: The Physical Science Basis. Contribution of Working Group I to the Fifth Assessment Report of the Intergovernmental Panel on Climate Change*, edited by: Stocker, T. F., Qin, D., Plattner, G.-K., Tignor, M., Allen, S. K., Boschung, J., Nauels, A., Xia, Y., Bex, V., and Midgley, P. M., Cambridge University Press, Cambridge, United Kingdom and New York, NY, USA, 2013.
- Stohl, A., Hittenberger, M., and Wotawa, G.: Validation of the Lagrangian particle dispersion model FLEXPART against large-scale tracer experiment data, *Atmos. Environ.*, 32, 4245–4264, 1998.
- Stull, R. B.: Similarity theory, in: *An Introduction to Boundary Layer Meteorology*, Springer Netherlands, 347–404, 1988.
- Taylor, J.: *An Introduction to Error Analysis: The Study of Uncertainties in Physical Measurement*, University Science Books, And ISBN: 093570275X (ISBN13: 9780935702750), 1997.
- Thum, T., Aalto, T., Laurila, T., Aurela, M., Hatakka, J., Lindroth, Anders, and Vesala, T.: Spring initiation and autumn cessation of boreal coniferous forest CO₂ exchange assessed by meteorological and biological variables, *Tellus B*, 61, 701–717, 2009.
- Tohjima, Y., Kubo, M., Minejima, C., Mukai, H., Tanimoto, H., Ganshin, A., Maksyutov, S., Katsumata, K., Machida, T., and Kita, K.: Temporal changes in the emissions of CH₄ and CO from China estimated from CH₄ / CO₂ and CO / CO₂ correlations observed at Hateruma Island, *Atmos. Chem. Phys.*, 14, 1663–1677, doi:10.5194/acp-14-1663-2014, 2014.
- Vaghjiani, G. L. and Ravishankara, A. R.: New measurement of the rate coefficient for the reaction of OH with methane, *Nature*, 350, 406–409, 1991.
- Wang, B.-R., Liu, X.-Y., and Wang, J.-K.: Assessment of COSMIC radio occultation retrieval product using global radiosonde data, *Atmos. Meas. Tech.*, 6, 1073–1083, doi:10.5194/amt-6-1073-2013, 2013.
- Wang, G., Huang, J., Guo W., Zuo, J., Wang, J., Bi, J., Huang, Z., and Shi, J.: Observation analysis of land-atmosphere interactions over the Loess Plateau of northwest China, *J. Geophys. Res.*, 115, D00K17, doi:10.1029/2009JD013372, 2010.
- Worthy, D. E. J., Chan, E., Ishizawa, M., Chan, D., Poss, C., Dlugokencky, E. J., Maksyutov, S., and Levin, I.: Decreasing anthropogenic methane emissions in Europe and Siberia inferred from continuous carbon dioxide and methane observations at Alert, Canada, *J. Geophys. Res.*, 114, D10301, doi:10.1029/2008JD011239, 2009.
- Yunck, T. P., Chao-Han, L., and Ware, R.: A history of GPS sounding, *Terr. Atmos. Ocean. Sci.*, 11, 1–20, 2000.